

Compressible Modal Instability Onset in an Aerodynamically Mistuned Transonic Fan

Christoph Brandstetter*, Benoit Paoletti and Xavier Ottavy

Univ Lyon, Ecole Centrale de Lyon
Laboratoire de Mecanique des Fluides et d'Acoustique - UMR CNRS 5509
F-69134 France
christoph.brandstetter@ec-lyon.fr

This paper describes observed modal oscillations arising from a feedback mechanism between an acoustic resonance in the exit flow channel and aerodynamic and aeroelastic disturbances in a transonic fan stage. During tests, the fan suffered from rotating stall and surge which were preceded by low frequency pressure fluctuations. Through a range of aerodynamic and aeromechanical instrumentations, it was possible to determine a clear chain of cause and effect, whereby geometrical asymmetries trigger local instabilities and modal oscillations through an interaction with the system acoustics. To the authors knowledge, this is the first time that modal oscillations occurring before stall are attributed to multi-physical interactions, showing that acoustic characteristics of the system can influence the aerodynamic as well as the aeromechanical stability of fans. This bears implications for the stability assessment of fans and compressors because firstly, the stability margin may be affected by standing waves generated in bypass ducts or combustion chambers and secondly, geometrical variations of the rotor blades which are believed to be beneficial for aeromechanical stability may lead to complex coupling phenomena.

INTRODUCTION

Intense research on the fundamental effects leading to the onset of instability in compressors and fans has been carried out during the past decades. At highly loaded conditions a strong interdependency of aerodynamics, mechanics and acoustics is present. Although models considering each of the sub-disciplines individually have been successfully validated and applied, modern simulation approaches fail to accurately predict periodic and transient phenomena in the highly coupled system. The interdependence of multi-physical effects is emphasized by the characteristics of lightweight rotor designs, particularly when composite materials are involved. In order to develop accurate prediction methods, it is necessary to provide comprehensive experiments from representative test vehicles.

To examine multi-physical interactions, a novel test fa-

cility has been established at Ecole Centrale de Lyon in a co-operation between LMFA and SAFRAN Aircraft Engines in 2017. Within this paper, the first results generated on this test rig, containing a scaled fan stage of a modern direct drive engine for civil aircraft are presented. The rotor assembly consists of carbon-fiber blades embedded in an engine-like intake section. With an initially unknown instability behavior, the stage was equipped with various unsteady instrumentation to resolve aerodynamic and acoustic signatures as well as structural reactions of rotor and facility. Particularly the route to onset of instability at highly loaded conditions lies in the focus of this investigation. As shown in the present paper, the machine under investigation shows a clear tendency towards modal stall inception that are affected by acoustic interactions with the facility.

Today it is well known that the inception of rotating stall, providing an inevitable breakdown of stable operation, is typically preceded by aerodynamic precursors of different characteristic length-scales and propagation speeds [1]. Major progress concerning long-length-scale perturbations or modes has been achieved in the 1980s with a model developed by Moore and Greitzer (e.g. [2], [3], [4]). Their two-dimensional model is capable to predict the evolution of small-amplitude pre-stall perturbations into significant disturbances that eventually form a stall cell and has proven accurate for low-speed machines. The predicted modes have been experimentally detected by different authors (e.g. McDougall et al. [5], Garnier et al. [6]). A study presented by Tryfonidis [7] on multiple low- and high-speed compressors showed that in low-speed applications incompressible, circumferentially propagating modes are dominant whereas a compressible mode appears at transonic conditions. For the incompressible modes, the phase velocity typically amounts to a fraction of the rotor speed whereas the compressible mode is associated to a disturbance that remains fixed to the rotor. Comparable results have been obtained by Bright et al. [8], who detected strong pre-stall disturbances traveling with the rotor speed already several thousand revolutions before stall. They found that during this period strong modal

pressure oscillations with a frequency of approximately 10% of the rotation frequency occur, which are eventually superimposed by short-length scale disturbances, also called spikes.

These spikes (e.g. [9], [10], [11], etc) are understood as small-scale radial vortices, which separate from the blade leading edge and propagate towards the subsequent rotor blade. The flow structure of these disturbances was predicted in 2000 by Inoue et al. [12]. In low-speed machines and particularly in rotors with large tip clearance ($> 1\%$ chord) the propagating leading edge separations lead to broadband pressure oscillations which have been discussed as "rotating instabilities" ([13], [14]) or part-span rotating stall ([15] and discussion).

In high speed machines Non-Synchronous-Vibrations may result from a forcing mechanism initiated by these propagating radial vortices whose occurrence resonates with a structural vibration mode of the rotor ([16], [17]).

The susceptibility of a specific machine to either modal or spike-type stall inception depends on the slope of the total-to-static compressor characteristic near stability limit, as presented by Camp and Day in 1998 [1]. The authors could trigger the respective breakdown mechanism in a multistage-machine with the stator setting, influencing the critical rotor incidence that is finally forcing the separation of flow at the leading edge.

Thus, today the convective short-length-scale stall precursor is physically widely understood, even though accurate simulations are still demanding (e.g. Pullan et al. [18], Yamada et al. [19]).

Compressible modifications of the Moore-Greitzer model have been applied and helped to characterize the shape of a modal disturbance that is predominant in high-speed compressors [20]. The fundamental understanding of their physical source and their sensitivity towards engine and facility parameters is still insufficient.

Since the rotor under investigation shows signatures of all described instability phenomena, a comprehensive analysis with distributed instrumentation has been carried out. The results indicate that the geometrical asymmetry of the rotor blades plays an important role for the modal pre-stall oscillations. Particularly an unstable behavior of individual blades that show significant manufacturing inhomogeneities is observed, which can be associated to a mechanism described by Wilson et al. [21]. In the present study we focus on the characterization of pre-stall signatures regarding the following objectives:

1. What is the particular physical manifestation of the propagating disturbance?
2. Are coherent aeroelastic or aeroacoustic interactions involved?
3. Which parameter determines the occurrence, amplitude and frequency of observed modal oscillations?

To comprehensively present the outcomes of the experiments, the paper is structured as follows:

After a brief description of the setup and the used methods we present general aerodynamic observations showing

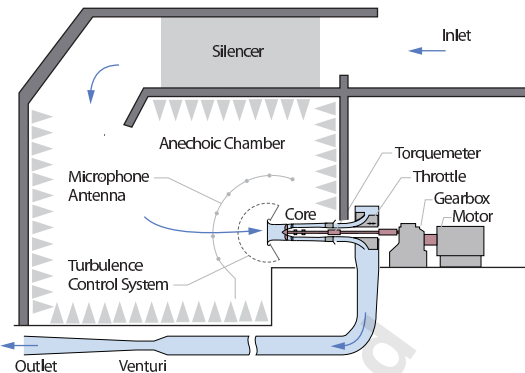


Fig. 1: TEST FACILITY SCHEMATIC

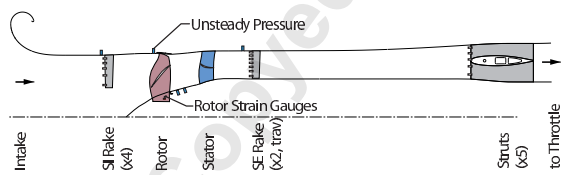


Fig. 2: FACILITY CORE SCHEMATIC

modal pressure oscillations as precursors of rotating stall for various rotation speeds. The parameters of the facility that determine the modal frequencies are derived from an acoustic study.

Finally we present a detailed analysis of the mechanical and aerodynamic reactions in the fan stage to derive the chain of course and effect for the observed modal resonance. The specific procedure comprises a) the isolation of unsteady phenomena; b) the identification of propagating disturbances by cross-correlating circumferentially distributed sensors; c) the quantification of aerodynamic asymmetries in the rotor.

With the applied analysis procedure it is possible to identify the geometrical parameter responsible for the characteristic instability behavior of the investigated setup.

Experimental Setup

The fan under investigation is a modern high-bypass carbon-fiber design derived from the CFM International LEAP engine. It is operated in the novel test facility ECL-B3 that is capable of electrically driving the stage in an anechoic chamber at transonic conditions with a maximum shaft power of 3 MW in an open loop. Through a set of silencers air is sucked in from the roof as shown in Fig. 1. The core consists of an engine-like inlet, followed by the fan stage that is supported by a very long hub (Fig. 2). The design allows future investigations of the interaction with an engine pylon which can be inserted in the space between stator and struts. To reduce complexity, the setup does not separate bypass and core flow. Instead, the original stator has been modified to provide comparable conditions at the rotor exit with a singular flow channel. The configuration has been in-

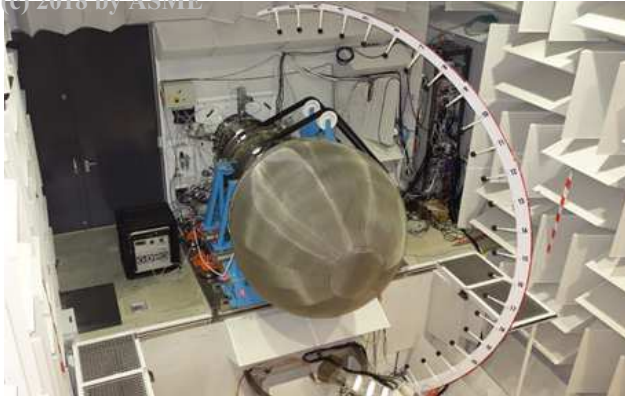


Fig. 3: FAN STAGE IN ANECHOIC CHAMBER; INSTALLED TURBULENCE CONTROL SYSTEM; ROTATABLE MICROPHONE ANTENNA

tentionally designed to reduce acoustic interactions with the downstream struts. After passing emergency bleed valves the compressed air reaches an axisymmetric cone-throttle and a subsequent collector box. The whole flow-section between fan-stage and throttle is equipped with acoustic liners. In order to accurately measure the mass flow, a Venturi-nozzle is installed after a 25m long circular tube section. Through a diffuser and another set of silencers the air is extracted to ambient conditions.

Machine and test rig are instrumented with more than 800 sensors (pressure, temperature, vibrations) which provide not only the global performance of the fan stage but also space- and time-resolved data. Upstream and downstream of the stage traversable sections allow circumferentially resolved flow field measurements. In addition to 180 microphones implanted within the machine, an acoustic antenna with 19 microphones is installed in the anechoic chamber (shown in Fig. 3) and can be rotated around the air intake of the machine to characterize the sound generated by the fan.

For the measurements presented in this paper, four flush mounted wall pressure transducers upstream of the rotor section distributed around the circumference ($\Theta = 30^\circ, 60^\circ, 144^\circ, 264^\circ$) are used to detect the propagation speeds of aerodynamic disturbances (Fig. 2). Signals of strain-gauges on the rotor blades were evaluated to measure structural waves in the rotor assembly. In comparison, coherent aero-mechanical interactions can be derived.

Signal Evaluation Methods To isolate non-periodic fluctuations, the deviation of the temporal pressure signals (also applicable for strain gauge signals), Δp is considered. This is determined by subtracting the ensemble average of the preceding r revolutions from the instantaneous pressure $p(i, n)$ at sample i and revolution n :

$$\Delta p(i, n) = p(i, n) - 1/r \sum_{m=1}^r p(i, n-m) \quad (1)$$

This method has been repeatedly applied to decorrelate the synchronous fluctuations and is comparable to "whitening" (spectral normalization) of a signal, but more comprehensive for this specific application (Young et al. [11] e.g. used the method to isolate the signature of a radial vortex from wall pressure data).

A procedure to automatically derive the propagation speed of disturbances, cross-correlations between circumferentially distributed sensors are performed for each revolution of a transient test (exemplarily, Garnier et al. [6], McDougall et al. [5] or Schreiber et al. [22] used this method for the characterization of pre-stall disturbances). The cross-correlation $p_1 * p_2$ between sensors 1 and 2 for example, is given by eq. 2:

$$p_1 * p_2(j) = \frac{1}{I} \frac{1}{\bar{\sigma}(p_1)\bar{\sigma}(p_2)} \sum_{i=0}^{I-j-1} \Delta p_1(i) \Delta p_2(i+j) \quad (2)$$

where I is the number of samples per revolution. For the presented results signals have been normalized with the average pre-stall standard deviation $\bar{\sigma}$. Each phase-shift, j , can be related to a propagation velocity c_{prop} in the absolute frame of reference. Expressed as a fraction of the rotor speed ΩR , this velocity becomes:

$$\frac{c_{prop,12}}{\Omega R} = \frac{\Delta\Theta_{12}/360^\circ}{j/I} \quad (3)$$

Using a single pair of sensors, the method has been extensively reported in literature. If multiple permutations of distributed sensors are used to calculate a minimum correlation over a revolution it is possible to reduce the amplitude of aliased correlation peaks [17]. It is necessary to interpolate the results onto a common propagation velocity vector due to the different sensor spacings. We applied this procedure to non-rotating aerodynamic and rotating structural instrumentation, which allowed to derive coherent interactions. The proposed method can be universally applied to distributed instrumentations and neither requires arbitrary adjustment parameters nor filters. In [17] it was possible to derive the weak pre-stall spike propagation velocity by application of this method. In the currently presented case, the propagation velocity of occurring stall cells is robustly and accurately detected in both the pressure and vibration signals. Furthermore it is possible to clearly characterize the pre-stall disturbance associated to the modal oscillation which is not a convectively propagating phenomenon as observed in [17].

RESULTS

General Unsteady Aerodynamics

Repeated investigations of the fan stage have been performed near stability limit based on the same procedure at different subsonic and transonic speedlines. The stage was stabilized for several minutes at a highly loaded operating point whereupon the exit throttle was sequentially closed at a very low and constant rate until surge or rotating stall was acoustically detected, leading to the opening of emergency valves. The transient recording of the pneumatic instrumentation (sampled at 1Hz) presented in Fig. 4 shows that the slope of the total-to-static pressure characteristics is comparable for all investigated speeds. At stall onset, the slope is close to zero but does not become positive (compare Camp and Day [1]).

Results of synchronously recorded unsteady aerodynamic and structural measurement systems for these operating speeds are presented in the following.

The unsteady casing wall pressure signal upstream of the rotor shows a clear signature of a rotating single stall cell for all investigated operating conditions between 80% (N80) and 105% of design speed. The behavior of the machine after initiation of a rotating stall cell varies depending on the rotation speed. As can be seen in Fig. 5, the period of rotating stall is followed by a low frequency oscillation of a characteristic (mild) surge shape for the speeds 90%, 100% and 105%. The frequency of surge oscillation approximates 10.5Hz for all measured speedlines. At 80%, 85% and 95% speed the stage enters rotating stall without any subsequent modulation that resembles a surge cycle.

As comprehensively discussed in literature a surge cycle consists of a period of rotating stall succeeded by a mass-flow breakdown and recovery (e.g. [23], [24]). In the present paper, we will focus of the precursors, observed before stall initiation.

For all speedlines, rotating stall is preceded by low frequency modal oscillations. Between 90% and 105% they are clearly visible as an envelope of the unsteady pressure signal (Fig. 5). The initiation of a rotating stall cell always occurs at a static pressure peak at $t=0$, corresponding to a minimum of axial velocity.

Low Frequency Stall Precursors

Regarding the low frequency spectra of the pre-stall wall pressure signals upstream of the rotor in Fig. 6 a) a common behavior for the high speedlines 90% to 100% is apparent. Frequency peaks around 9Hz and 14 Hz as well as their harmonics are observed depending on the speedline. The frequency resolution is low due to the small fft-window of 0.8s that has been used to derive the temporal evolution presented in Fig. 6 b). During the last 2-4 seconds before the first rotating stall cell the amplitude of an oscillation at approximately 14 Hz rises continuously from below 1% to 5% of the average dynamic pressure at the intake as can be seen in the modal amplitude graphs (Fig. 6 b)). At N105% the oscillation already appears multiple seconds before stall with varying amplitude of up to 10% of the dynamic pressure at

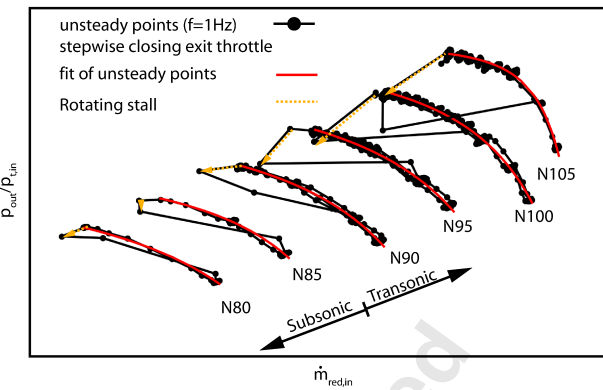


Fig. 4: MEASURED FAN STAGE CHARACTERISTICS FOR SUBSONIC AND TRANSONIC SPEEDLINES

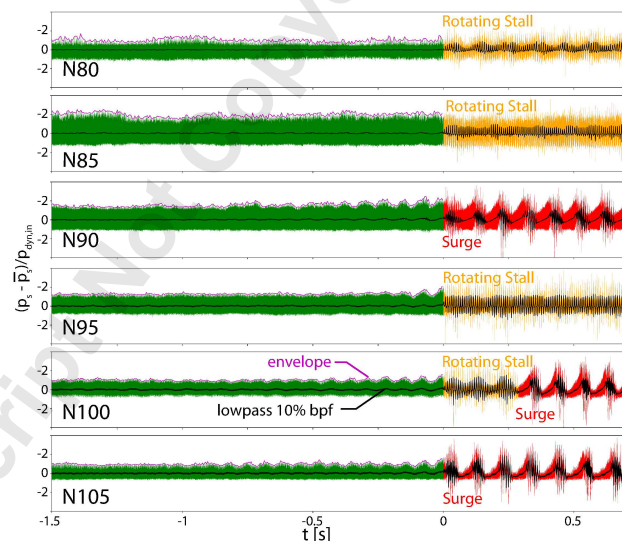


Fig. 5: TIME HISTORY OF UNSTEADY WALL PRESSURE UPSTREAM OF THE ROTOR FOR ALL MEASURED SPEEDLINES, STALL ONSET AT $T=0$

the intake. In contrast, the amplitude of the 9 Hz mode and their harmonics remains constant until rotating stall (occurring at $t=0$).

The comparison of different instrumentations presented in Fig. 7 shows that the relative amplitude of the 14Hz oscillation is dominant for the casing wall pressure, both upstream and downstream of the stage. The influence on torque and axial force rises to approximately 0.25% of the average value at near stall conditions. Distributed accelerometers prove that casing and hub oscillate synchronously.

Summarized, the observed 14 Hz oscillation is a planar pressure wave that continuously increases several seconds before stall to an amplitude of 5-10% of the dynamic inlet pressure (zero-to-peak). It causes significant reactions of the machine and reaches always a pressure peak just before the first rotating stall cell occurs. The actual frequency rises with the speed of sound in the exhaust system (accord-

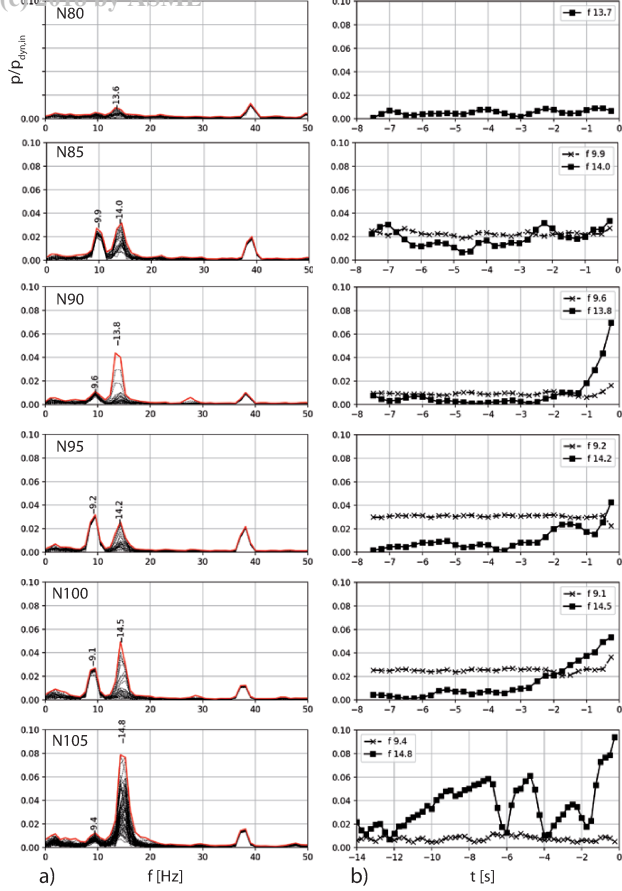


Fig. 6: PRE STALL SPECTRUM AND TEMPORAL EVOLUTION OF SELECTED MODAL AMPLITUDES, SLIDING FFT-WINDOW 0.8S, HANNING, 50% OVERLAP

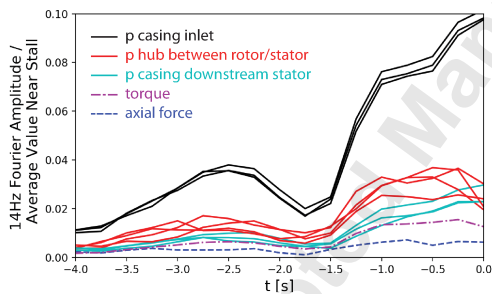


Fig. 7: 14HZ MODE AMPLITUDE IN DIFFERENT INSTRUMENTATIONS FOR N105%

ing to the temperature on the respective speedline) from 13.6 Hz at 80% speed to 14.8 Hz at N105%. For convenience we refer to the oscillation as the 14 Hz Mode in the following.

Acoustic Response of Exhaust System

An acoustic analysis of the machine exhaust including the ring diffuser has been carried out to determine the source for the observed pressure oscillations which occur at fre-

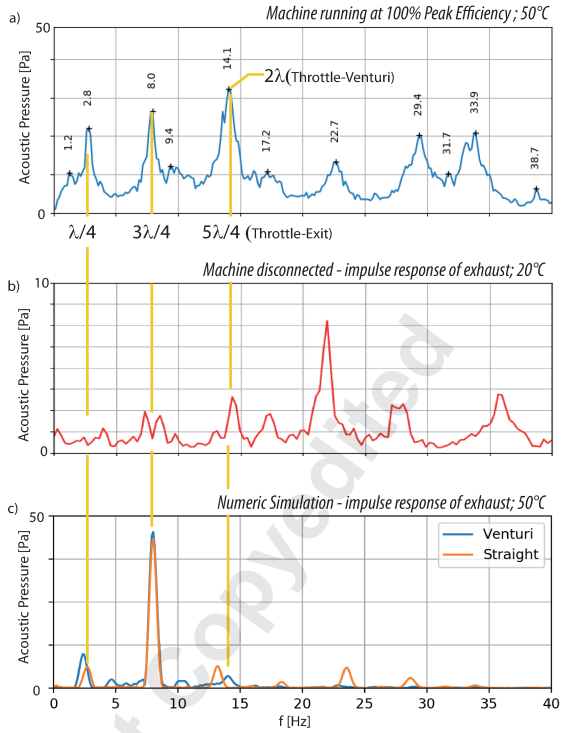


Fig. 8: ACOUSTIC SPECTRUM OF EXHAUST, EXPERIMENTAL AND NUMERICAL RESULTS

quencies far below the rotation speed (200 Hz to 260 Hz depending on the speedline). Three different studies have been carried out: a) acoustic measurements in the exhaust with the machine running at N100%; b) measurements of the response of the isolated exhaust and throttle system to an acoustic impulse generated by small explosive charges; c) numerical simulations of the exhaust system. These three approaches gave results presented in Fig. 8.

The frequency spectrum of a microphone downstream of the machine throttle at a stable operating point (100% Speed) is shown in Fig. 8 a). The first fundamental acoustic modes of the exhaust pipe are clearly visible at 2.8 Hz and 8 Hz, which correspond to a $\lambda/4$ and $3\lambda/4$ standing wave with an open termination at the exit and an approximately closed termination at the throttle. Higher modes attributed to the open exit termination of the system can also be determined from the spectrum. To confirm that the observed spectra are independent from the machine core, repeated impulse responses of the exhaust system using an explosive noise source have been recorded, showing the spectrum presented in Fig. 8 b). All modes observed with the machine running at 100% can be found in the isolated spectrum, particularly the 14Hz Mode, even though the frequency resolution is much lower because only segments of 3 seconds after each impulse could be used for the analysis.

To support the analysis, coarse simulations have been set up in Ansys CFX with essential parameters given in Fig. 9. Since the simulations are not used for the interpretation of the presented mechanisms in the fan stage but rather for a qual-

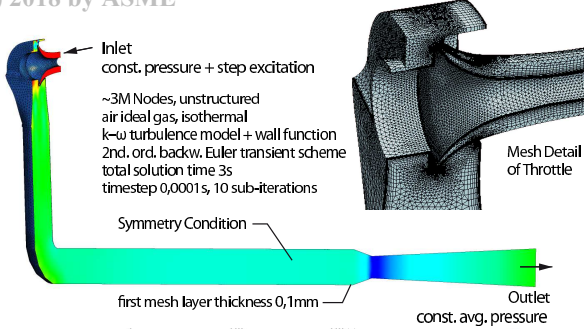


Fig. 9: GEOMETRY AND PARAMETERS OF NUMERICAL SETUP

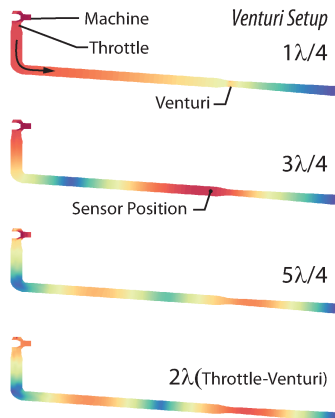


Fig. 10: SHAPE OF LOW FREQUENCY ACOUSTIC MODES (MODAL PRESSURE AMPLITUDE); NUMERICAL RESULTS AT DESIGN MASS FLOW

itative interpretation of the acoustic modes, further details are omitted for brevity. In contrast to high-frequent acoustic interactions between blade rows (e.g. [25]), the observed modes of the exhaust system are robustly predictable.

The numerical results of the exhaust system confirm the analytical interpretation of the observed modes in the spectra depicted in Fig. 8 c). The fundamental modes at $\lambda/4$ and $3\lambda/4$ observed in the measurements are well represented. The comparison of a simulation with and without Venturi nozzle shows that the $5\lambda/4$ resonance of the straight section appears around 13 Hz and is shifted towards 14 Hz with installed nozzle. The modeshape indicates a 2λ oscillation between throttle and Venturi-Nozzle and explains the broadness of the 14Hz peak in Fig. 8 a). All fundamental mode shapes derived from the simulations are presented in Fig. 10.

This analysis clearly demonstrates that the acoustic characteristics of the exhaust system determine the frequencies observed at near stall conditions because all peaks can be clearly associated to fundamental acoustic modes. To investigate how the respective modes are excited and resonate with the fan stage further instrumentations are analyzed in the following.

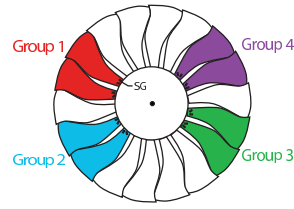


Fig. 11: ROTOR STRAIN GAUGE INSTRUMENTATION

Mechanical Reactions of the Rotor Blades

The rotor is instrumented with strain gauges (SG) sensitive to the fundamental blade modes which are transferred via telemetry. Four groups of neighboring blades are instrumented as depicted in Fig. 11 with two redundant sensors per blade. A spectrogram of one sensor during a transient throttling procedure into rotating stall and surge is shown in Fig. 12 a) with the pre-stall maximum value attached to the right. The spectrogram of raw data reveals significant forced response at all Engine-Order harmonics, particularly at EO 4, which is very close to Blade Mode 3 at the shown operating speed. After subtracting the sliding ensemble average of each 10 revolutions from the raw data, the synchronous excitation disappears from the spectrogram, shown in fig 12 b). The unsteady response during stall onset at $t=0$ is still clearly present. This point is relevant because the unsteady signal is used for the cross-correlations presented in section "Coherent Propagating Disturbances". This representation proves that neither Flutter nor Non-Synchronous-Vibrations linked to the blade eigenmodes are present before rotating stall occurs. If there were any significant pre-stall amplitude rise due to an aeroelastic instability of a fundamental blade mode (such as NSV) it would be clearly depicted in this plot (compare [17]). Instead, the pre-stall amplitudes of all modes remain below 10% in relation to the average amplitude of Blade Mode 1 during rotating stall (\overline{SG}_{Norm}).

Subcritical pre-stall excitations of the blades at the formerly discussed acoustic low-frequency modes (Engine Order <0.05) are observed, showing clear peaks in the pre-stall strain gauge spectrum presented in Fig. 13. The exciting pressure waves are planar, hence no Doppler-shift is observed in the rotor system.

To analyze the interaction with the low-frequency pressure oscillation, the strain gauge data has been bandpass filtered, revealing an unexpected pattern presented in Fig. 14. The graphs on the left hand side show the filtered signals, the envelope is attached to the right. The bandpass-filtered data around the 14 Hz oscillation (+1Hz butterworth, 2nd deg, frequency adjusted to actual speed of sound) presented in Fig. 14 a) exhibits that the different instrumented blade groups (comp. Fig. 11) react in local coherence to the disturbance. Each blade is instrumented with two gauges, proving the significance of this finding.

Several seconds before rotating stall occurs, the blades of a local group show a similar beating amplitude, whereas the different groups act independently and temporarily drift out of phase (e.g. Fig. 14 a) at $t=-1.8s$).

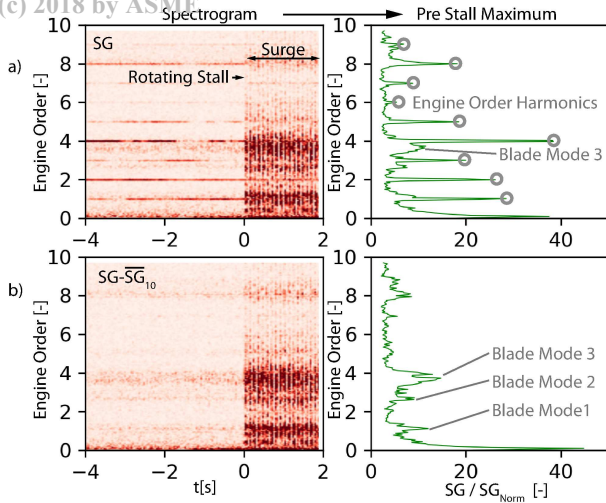


Fig. 12: STRAIN GAUGE SPECTROGRAM AND PRE-STALL MAXIMUM; A) RAW SIGNAL; B) SIGNAL WITH SUBTRACTED SLIDING ENSEMBLE AVERAGE OF EACH 10 REVOLUTIONS; N105

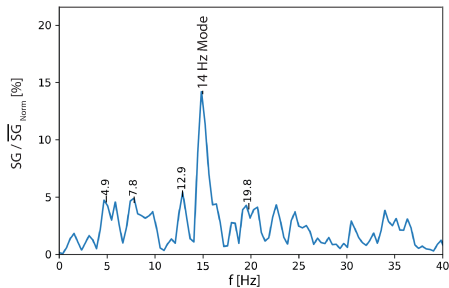


Fig. 13: LOW FREQUENCY SPECTRUM OF ROTOR STRAIN GAUGES; AVERAGE OF LAST 2 SECONDS BEFORE ROTATING STALL; N105

Group 1 (red) is most susceptible to the low frequency pressure oscillation. Within the last second before rotating stall, all groups react in phase to the 14 Hz Mode disturbance and show a continuous amplitude rise that reaches about 20% of the first bending mode amplitude during rotating stall.

The same pattern of circumferential asymmetry in the rotor is visible when regarding a low-pass filter below 10 Hz, shown in Fig. 14 b).

Both oscillations can be associated to the acoustic modes formerly described and are far below natural frequencies of the structure. The high amplitude indicates a strong forcing whereas the severe asymmetry has not been anticipated due to the planar pressure disturbance. This point will be addressed discussed in section "Aerodynamic Asymmetry".

Bandpass-filters around the first three blade-eigenmodes (Fig. 14 c), d) and e)) confirm, that the pre-stall response shows no signature of flutter or NSV (Similar results for higher order modes). Nevertheless, the amplitude of the

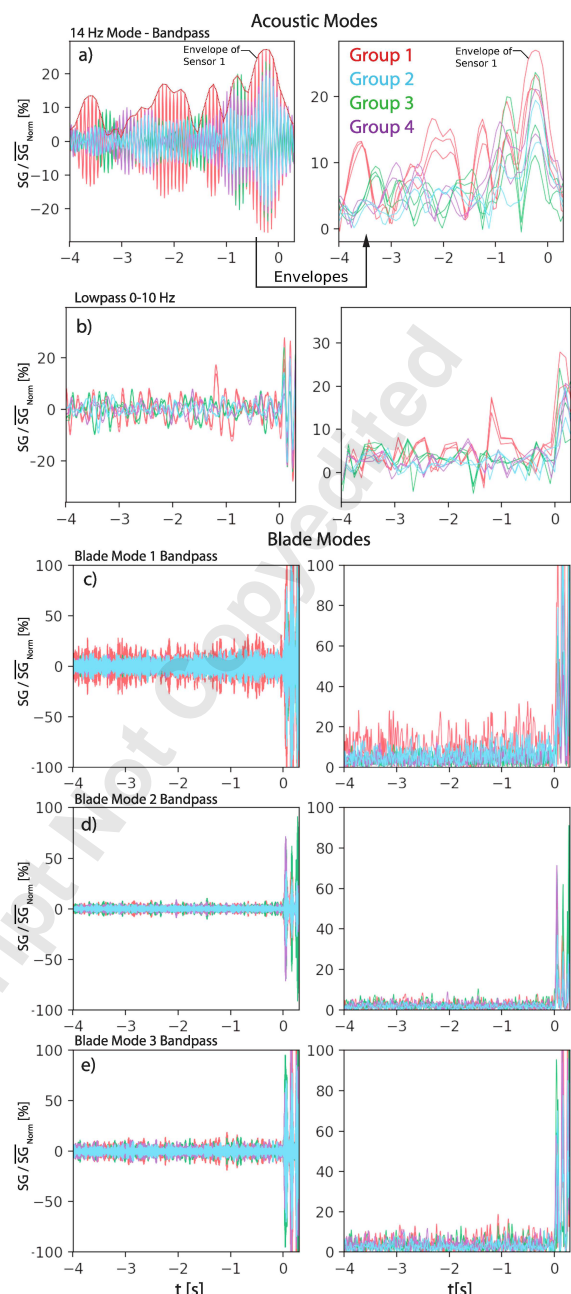


Fig. 14: BANDPASS FILTERED STRAIN-GAUGE DATA FOR N105; NORMALIZED WITH AVERAGE AMPLITUDE OF BLADE MODE 1 DURING ROTATING STALL; ENVELOPES ON THE RIGHT REPRESENTING THE CONNECTION OF ADJACENT PEAKS IN THE BAND-PASS FILTERED SIGNAL OF EACH SENSOR

first eigenmode (flap- or bending mode) is prominent for the blades of group 1 (red) and of the same order of magnitude as the 14 Hz reaction.

Thus, the present rotor does not develop a coherent pattern during the pre-stall period that is circumferentially propagating relative to the rotor (Nodal-Diameter). Instead, a severe asymmetry of the mechanical reaction is observed asso-

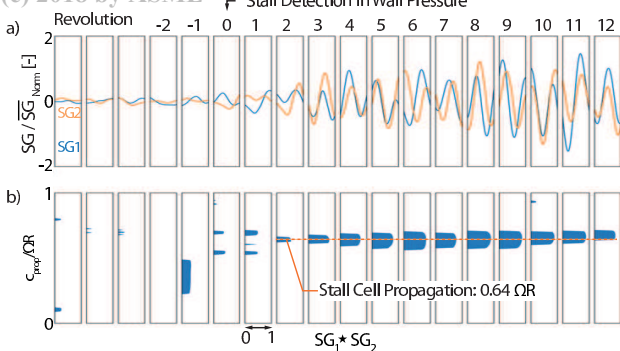


Fig. 15: STRAIN GAUGE SIGNALS OF DIFFERENT ROTOR BLADES DURING STALL ONSET; RESULTING CROSS-CORRELATION PEAKS DEPENDING ON PROPAGATION SPEED; N105%

ciated to the low-frequency pressure disturbance.

Coherent Propagating Disturbances

To prove the absence of a propagating mode in the rotor, cross-correlations between the different instrumented blades have been calculated. This allows to detect the propagation speed of a structural disturbance. Exemplary, Fig. 15 a) shows the unsteady signals of two strain gauges on different blades during the onset of rotating stall that has been detected in the unsteady pressure signal in revolution 0. The graphs show intense reactions of the rotor blades which are induced by the propagating stall cell.

The corresponding cross-correlation $SG_1 * SG_2$ is plotted against the respective propagation speed $c_{\text{prop}}/\Omega R$ in Fig. 15 b). The cross-correlation has been calculated for all permutations of instrumented blades, excluding redundant sensors. The temporal evolution of the minimum value of these correlations is presented in Fig. 16 a) with the propagation speed in the absolute frame of reference on the ordinate. Starting from the initiation of rotating stall in revolution 0 this plot clearly depicts the propagation speed of the stall cell of 64% rotor speed in the absolute frame of reference. At the shown 105% speedline a surge cycle with intermittent stall periods develops rapidly, visible between revolutions 0 and 500.

Before the onset of rotating stall, no clear indication for coherent propagating disturbances are observed. Lower-amplitude peaks occur randomly before stall at a propagation speed between 0-0.3ΩR, representing synchronous impulse-like disturbances of the periodic signal visible in all blade pair correlations.

The same method of permuting cross-correlations has been applied to the unsteady wall pressure signals close to the leading edge, yielding the results shown in Fig. 16 b). For the period after stall-onset the results are almost identical to the strain-gauge signal, proving a strong coherence between the aerodynamic excitation and the structural response. Yet, this coherence is only present for the stall period. During the

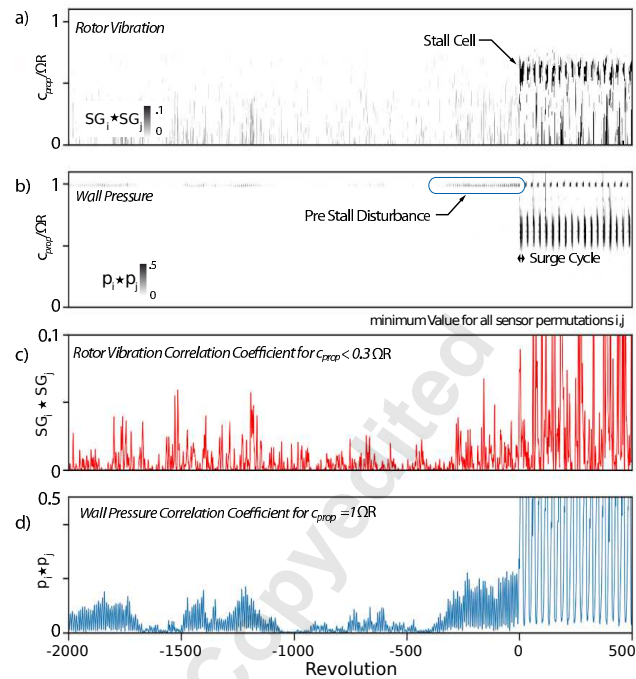


Fig. 16: COMPARISON OF PROPAGATING STRUCTURAL AND AERODYNAMIC DISTURBANCES FOR 105% SPEEDLINE; PROPAGATION SPEED IN STEADY FRAME OF REFERENCE

pre-stall period, the results show that strong deviations from the periodic signal with propagation speed close to $1\Omega R$ continuously increase within the last 400 revolutions. These inhomogeneities are fixed to the rotor and each remain over at least one revolution since they were observed with all circumferentially distributed pressure sensors.

The appearance of aerodynamic and mechanical disturbances during the pre-stall phase is not clearly coherent. The comparison of the maximum value of the structural disturbance between 0-0.3ΩR in Fig. 16 c) with the rotor fixed aerodynamic disturbance in Fig. 16 d) only reveals that the strongest mechanical impulses are measured during phases of intense aerodynamic inhomogeneities.

Comparable results have been obtained for the lower speedlines. The rotor fixed disturbances always occur during the final phase before the onset of rotating stall. The relative intensity of the disturbance increases with the rotor speed. The intermittent amplitude rise visible in Fig. 16 d) was only observed for the 105% speedline (compare Fig. 6).

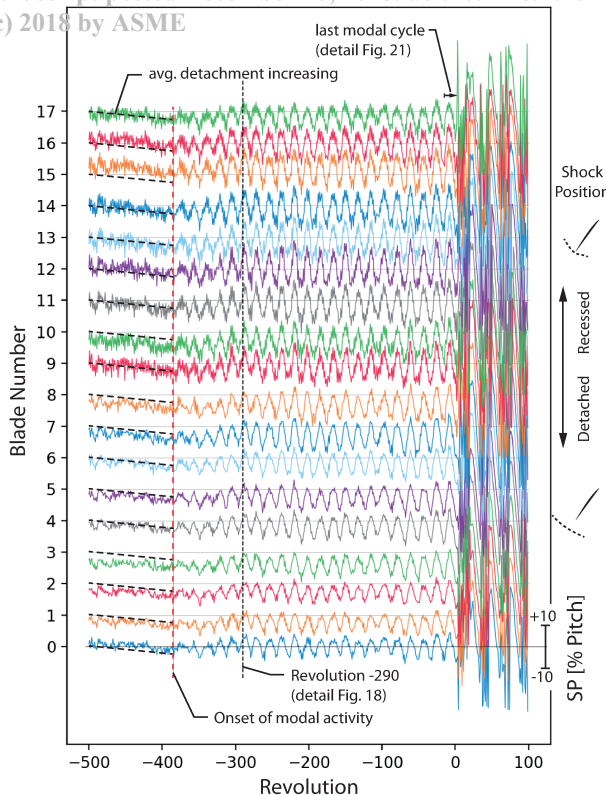


Fig. 17: VARIATION OF SHOCK POSITION FOR N105%;
DETECTED WITH UNSTEADY PRESSURE SENSOR
UPSTREAM OF ROTOR LEADING EDGE

Aerodynamic Asymmetry

To characterize the aerodynamic disturbance responsible for the correlation peaks in Fig. 16 a), the position of each leading edge shockwave relative to the rotor blade has been extracted from wall-pressure signals. Therefore, the pressure signal during one revolution has been divided into equal parts for each blade passing. The arrival time of each shock could then be robustly detected by calculating the cross-correlation of individual blade passing signals with a median signal at steady near stall conditions. Results for the 105% speedline are presented in Fig. 17, with each line representing the shock arrival time for the respective blade.

After a period of continuous shock detachment for all rotor blades between revolutions -500 and -390 a distinct low-frequency oscillation establishes around 390 revolutions ($\approx 1.5\text{s}$) before stall. The graph demonstrates that the average shock position and its variation is not homogeneously distributed over the rotor. Instead it is found that one section of the rotor is always working with a further recessed shock whose position is closer to the rotor blade (comp. sketch in Fig. 17). The effect is most severe for the blade numbers 9 to 16 which also suffer of the strongest fluctuations. It is also visible that Blade 15 already works with a further recessed shock before the onset of modal activity.

The time history of one wall-pressure sensor during this period is presented in Fig. 18 a) wherein the signature of

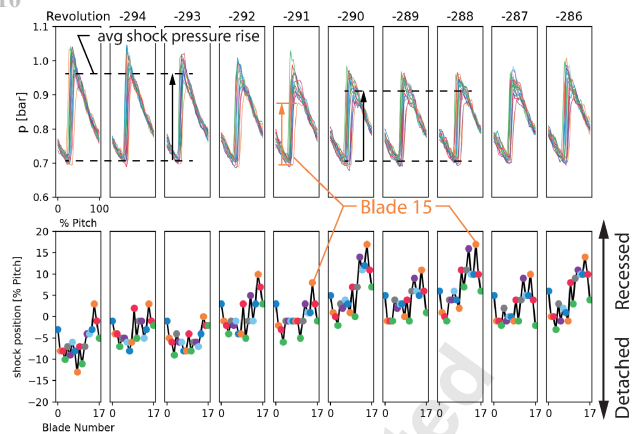


Fig. 18: SHOCK FLUCTUATION AROUND REVOLUTION -290 BEFORE ROTATING STALL; N105%

each blade passing is plotted against rotor pitch for several revolutions. Clearly the passage of the leading edge shock underneath the sensor depicts as a step. For revolutions -295 to -293 the average shock pressure rise is higher than for revolutions -290 to -288. Blade 15 always shows a recessed shock position associated to a significantly reduced pressure rise. The arrival time of the shock with respect to each blade is given in Fig. 18 b). It shows the same trends for the shock arrival time as a function of the blade number. The rotor goes from a state with homogeneous loading and high average shock pressure rise (before revolution -293) to a more asymmetric state of recessed and weak shocks that are non-uniformly distributed (starting from revolution -290). In all revolutions, Blade 15 is clearly prominent with the most recessed and weakest shock wave.

The comparison of all shown revolutions in Fig. 18 b) demonstrates the development of an asymmetrical load distribution that remains fixed with the rotor. In contrast to a spike type leading edge separation this disturbance is not propagating towards the subsequent blade before the onset of rotating stall but diminishes again periodically. The average, minimum and maximum shock position during the pre-stall phase is given in Fig. 19 a). The strongest fluctuations occur in the rotor sector containing the blades with recessed shock position (Blades 9 to 16). When comparing the measurements at different speedlines, it is found that the same blades are most susceptible to fluctuations of the shock-position and associated blade loading. The most recessed position reaches values steadily observed at peak-efficiency operation, a condition that should be more stable from an aerodynamic point of view. Nevertheless the results clearly show that the blades with recessed shock are aerodynamically more unstable.

Since no signs of propagating flow separations are observed, the reason for the unsteadiness of this configuration is assumed to rely on a non-linear fluid-mechanical interaction that is similar to the one presented by Wilson et al. [21], who have shown the influence of static stagger variability on the dynamic pressure untwist behavior of fan assemblies. At transonic conditions the untwist is essentially influenced by

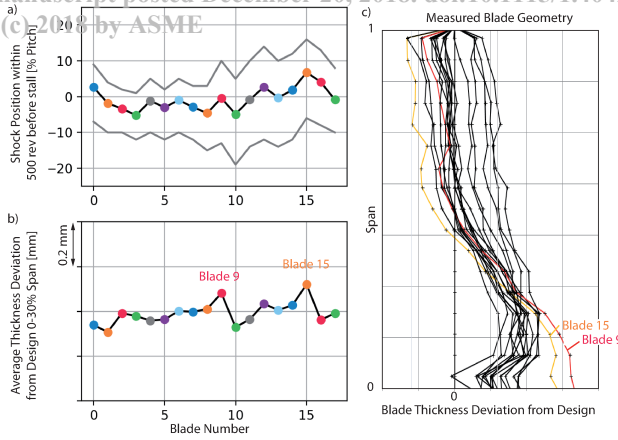


Fig. 19: COMPARISON OF SHOCK POSITION AND BLADE GEOMETRY PARAMETER

the position of the shock. If a blade works at started conditions with a swallowed shock and a supersonic zone around the leading edge, the untwist is significantly lower than for a detached shock configuration with subsonic flow at the pressure side. The divergence of the passages adjacent to the mis-staggered blade is asymmetric, influencing the lift distribution, particularly on the downstream blades [26]. In [21] a single mis-staggered blade provoked unstable conditions of the whole assembly with alternating started and unstarted passage flow. Such a configuration explains the lower shock pressure rise observed for the recessed shocks in Fig. 18. The actual stagger angle at the blade tip depends on the static geometry and the resistance of the individual blades towards pressure untwist, whereupon possible influential geometrical parameters of the measured blades have been analyzed.

A clear correspondence has been found between the shock position and the measured blade thickness of the lower 30% span, depicted in Fig. 19 b). Here, the blades with maximum foot thickness work with a less detached shock that fluctuates more than $\pm 10\%$ of the rotor pitch. The two blades 9 and 15 who show deviations from the design value shown in Fig. 19 c) are clearly prominent in the aerodynamic asymmetry over the whole pre-stall process. Further geometrical parameters are similarly correlated but additional measurements that allow the identification of unsteady untwist and the actual position of the shock on the blade suction side are necessary to derive the sensitivity of respective values. Nevertheless, the results clearly indicate that the aerodynamic mistuning is sufficient to provoke a significant unstable asymmetry in the loading distribution of the rotor.

The amplitude of asymmetry is modulated with a clearly dominant frequency of the 14 Hz mode for all speedlines as depicted in the spectrum in Fig. 20. Further peaks observed in the pressure spectra in Fig. 6 diminish, particularly the 9 Hz Mode.

The analysis demonstrates that the correlation peaks observed for $1\Omega R$ in Fig. 16 result from a circumferential inhomogeneity pattern of the respective shock position.

To understand the responsible modal resonance cycle,

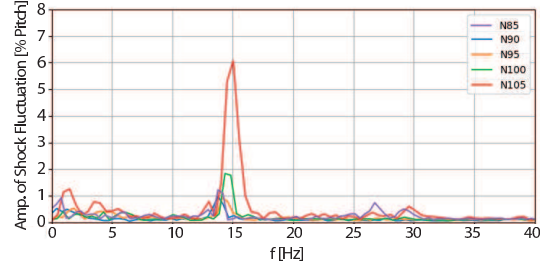


Fig. 20: SPECTRUM OF PRE STALL SHOCK FLUCTUATION FOR ALL TRANSONIC SPEEDLINES; AVERAGE VALUE FOR ALL BLADES DURING 2 SECONDS (≈ 500 REV.) BEFORE ROTATING STALL

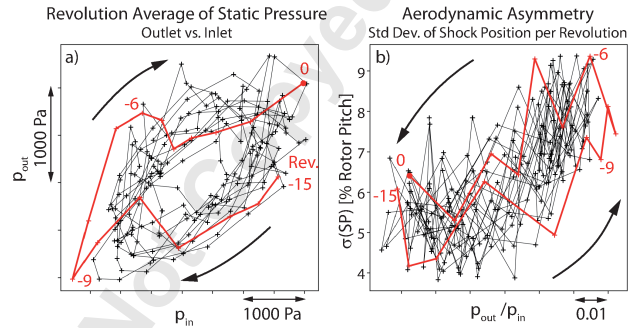


Fig. 21: MODAL CYCLE HYSTERESIS N105%; BLACK CROSSES SHOW REVOLUTION AVERAGE FOR LAST 10 MODAL OSCILLATIONS BEFORE ROTATING STALL; FINAL CYCLE IN RED

Fig. 21 shows measured values of the last 10 periods. The phase plot (a) of stage outlet pressure over inlet pressure is tracing clockwise. The last cycle shown in red starts at a point of high outlet pressure and high inlet pressure (Rev. -15). During this phase the shock inhomogeneity over the circumference (b) is low (5-6%). After a slight drop of outlet pressure, the inlet pressure decreases strongly leading to an increased stage pressure ratio due to high incidence (Rev. -9). At this point, the aerodynamic asymmetry grows until Rev. -6 and reaches a maximum at 9% standard deviation of shock position within one revolution. At this point the stage pressure ratio has reached a peak and starts to fall until revolution 0 where stall is initiated (comp. Fig. 5).

Hence, it is evident that it is not a flow separation mechanism that is resonating with the modal wave but a rotor-fixed asymmetry. Its amplitude is frequency- and phase-locking to the compressible (or acoustic) mode of the exhaust system. The asymmetry is strongest for the phase of maximum pressure rise and triggered by geometrical inhomogeneity influencing the unsteady untwist of the blades.

Interpretation

Comparing these results with the acoustic analysis of the exhaust, the pre-stall mechanism can be summarized as follows with an illustration in Fig. 22:

1. At highly loaded conditions, small geometrical inhomogeneities of the rotor blades cause asymmetrical loading distribution, Fig. 22 a).
2. The unsteady untwist of the rotor blades becomes eventually unstable for individual blades, in our case for those operating at unloaded conditions.
3. The asymmetry leads to a reduction of the average stage pressure ratio and a subsequent drop of the stage exit pressure that is emitted to the exhaust and develops to a planar wave. The circumferential asymmetry is reduced by the long tubing system.
4. The geometry of the exhaust system, specifically its acoustic property, causes a reflection of this pressure wave and determines a characteristic timescale (b).
5. With arrival of the reflected pressure wave in the fan stage remaining aerodynamic inhomogeneities in the rotor are amplified, leading to subsequent emissions of pressure waves to the exhaust (c)→(d). At transonic conditions singular passages temporarily develop started flow conditions with a supersonic zone at the tip of the pressure side (comp. [21] and [26]).
6. A closed feedback loop between the amplitude of aerodynamic asymmetry in the rotor and a standing pressure wave in the exhaust system establishes. The dominant frequency is according to the mode with highest eigenfrequency of the exhaust that is efficiently reflecting the incoming pressure disturbance. Obviously the amplification and reduction of aerodynamic asymmetry in the rotor requires a specific time, since the exhaust system might also resonate with higher order modes (comp. Fig. 8) but always locks on the 14Hz mode.
7. In the observed case the respective mode is associated to the section change at the Venturi-tube and a $5\lambda/4$ open exhaust termination resulting in a characteristic frequency of $\approx 14\text{Hz}$ (at 20°C).
8. The first two fundamental modes of the exhaust (3Hz and 9Hz) are also observed because of random excitation but are not in direct resonance with the rotor asymmetry.
9. Only planar waves are contributing to this process since the system geometry cuts off all modes with higher wave-numbers at the observed frequencies.
10. Immediately before rotating stall, a weak spike-type signature is observed within the last 2-5 revolutions to initiate the single stall cell.
11. This characteristic behavior has been observed at all transonic speeds from 90% to 105%.

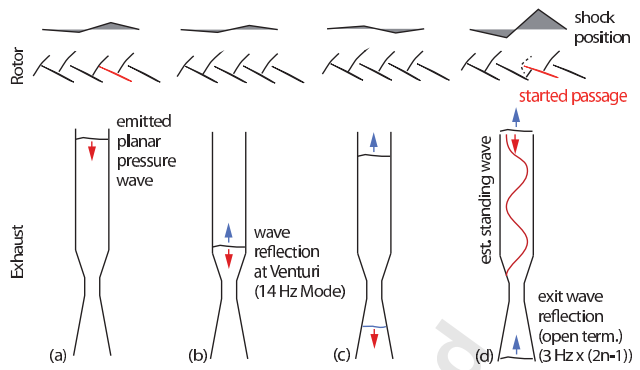


Fig. 22: FEEDBACK LOOP BETWEEN ROTOR ASYMMETRY AND EXHAUST

Discussion

The interpretation and evidence in the previous sections clearly demonstrate that an aerodynamic instability in a rotor stage can be driven by planar acoustic modes in the exhaust system. It furthermore shows that this can cause an aeromechanical response of the rotor blades which is non-linear and asymmetric and governed by geometrical variations between the rotor blades.

While the frequencies measured in this study are specific to the test facility, the existence of this acoustic, aerodynamic and aeromechanical interaction phenomenon bears implications for engineering applications. Planar acoustic modes can develop in the bypass duct and combustion chambers of engines. If one of the associated frequencies matches the aerodynamic response time of the rotor, resulting fluctuations can cause an unsteady untwist behavior adversely affecting the aerodynamic or aeromechanical stability boundaries.

These findings are particularly interesting, as blade-to-blade variations (i.e. mistuning) are usually considered beneficial for aeromechanical stability (i.a. [27], [28], [29], [30]). Through reduction of system symmetry the establishment of propagating modes leading to Fan-flutter or NSV can intentionally be attenuated. The presence of blades with started flow conditions will definitely suppress the circumferential propagation of separated flow structures near the blade leading edges [17].

The asymmetric untwist behavior, which was first studied by Wilson [21], and its amplification by acoustic modes described in the current work, presents a case where mistuning can cause or exacerbate aeromechanical oscillations.

Furthermore, the findings clearly show that the acoustic characteristics of the system must be considered to ensure transferability between computational predictions, rig tests and engine conditions. The authors generally suggest a thorough analysis of the acoustic properties of test-facilities used to investigate instability mechanisms in turbomachinery. Particularly concerning the low-frequent planar modes, reproducible spectra could be measured using explosive noise sources.

For the specific facility, the dominant acoustic mode re-

sults from the change of the flow channel diameter inside the Venturi-Tube from 1008mm to 650mm. This section change is associated to an acoustic reflection coefficient for planar waves of +0.41. Also, the Mach-Number between throttle and Venturi-Tube is low also at design conditions which results in a very weak acoustic damping, particularly for the low frequencies that are involved. Yet, the section change is necessary to provide the desired mass-flow measurement accuracy.

It is intended to apply a perforated section to reduce the exit-termination because geometrical limitations prevent the integration of a smooth exit treatment. In order to further attenuate the resonance of the exhaust system at its fundamental modes, Helmholtz-resonators which are tuned to the respective frequencies will be integrated as depicted in Fig. 23. Numerical and experimental pre-studies on a scaled setup (1/3) have shown that this configuration is capable to reduce the system resonance at the respective modes by 6dB to 9dB. It is envisaged to analyze both the sensitivity on the resonance frequency and the acoustic termination coefficient in future work. Furthermore, the research focus will lie on the positive aspects associated to the observed mistuning concerning rotating modes.

Summary

The presented study has shown that the acoustic properties of the facility strongly influence the instability behavior of the fan stage under investigation.

In the current setup stage loading at near-stall conditions is affected by standing waves in the exhaust system, which force a lock-in of aerodynamic effects in the rotor.

The specific mechanism is not of typical aeroelastic nature but results from an interaction between aerodynamic asymmetry in the rotor and acoustic feedback of the exhaust system.

The asymmetry is associated to aerodynamic mistuning of the rotor blades that is affecting the unsteady untwist behavior. In the observed case, blades with low untwist, operating with less detached shocks enter unstable flow conditions. Singular blades whose geometry slightly deviates from design enforce an unstable behavior of a large sector of the rotor.

During the pre-stall phase no propagating phenomena have been observed in the rotor. It is possible that the unintended aerodynamic mistuning of the rotor is sufficient to suppress convective propagations. Intentional application of the present non-uniformity might be a promising method to attenuate various instability mechanisms like NSV and Flutter.

The observed pre-stall oscillations resemble the compressible form of modal waves that have been repeatedly reported in literature. Because of the specific setup with a very long exhaust system only low-frequent planar waves are present. It is obvious, that the acoustic termination of a fan or compressor stage can provoke a phase and frequency lock-in of aerodynamic inhomogeneities which are then amplifying. For much shorter exhaust systems circumferentially

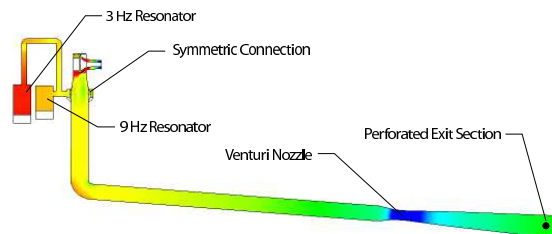


Fig. 23: INTEGRATION OF HELMHOLTZ RESONATORS TO REDUCE ACOUSTIC RESONANCE OF EXHAUST SYSTEM

propagating acoustic modes can be dominant and determine the occurrence of modal oscillations. The findings are directly transferable to a real engine whose duct system enables acoustic resonance of planar waves.

The high mass-flow measurement accuracy of the Venturi-Nozzle is highly valuable for performance measurements at stable conditions but affects the transient investigations. To enable accurate control of the stage loading it is intended to attenuate the resonant behavior of the exhaust system. It is envisaged to analyze both the sensitivity on the resonance frequency and the acoustic termination coefficient.

Extensive instrumentation has proven the capability of the novel test-facility to comprehensively investigate and interpret the highly complex instability mechanisms of a modern fan-stage. Particularly the identification of the source for modal oscillations observed before rotating stall onset contributes to the fundamental understanding of turbomachinery instability. Furthermore, the detection and quantification of aerodynamic asymmetry in the rotor depending on geometric inhomogeneity is highly valuable during the design process of future engines.

The presented results are promising for upcoming research programs with an open-test-case UHBR-Fan-stage that is currently under development at Ecole Centrale de Lyon and will be commissioned in 2019 with a specific focus on the effects of aerodynamic mistuning.

Acknowledgements

The assessment of the test-facility was enabled through financial supports of Agence Nationale de la Recherche (ANR, Project d'EquipEx PHARE) and Conseil pour la Recherche Aeronautique Civile (CORAC - Programme CUMIN). Buildings and infrastructure were supported by Ecole Centrale de Lyon (ECL), instrumentations supported by Institut Carnot (INGENIERIE@LYON - Project MERIT).

We are grateful for the continuous collaboration and financial support of SAFRAN Aircraft Engines since the beginning of this project and specifically for the present measurement campaign.

The authors would like to particularly acknowledge the previous contributions of Gilbert Halter, Lionel Pierrard, Pierre Laucher and Sébastien Gogoué.

Nomenclature

bpf	Blade Passing Frequency)
$c_{ax,in}$	Average Axial Velocity at Stage Inlet (Near Stall)
c_{prop}	Wave Propagation Speed (Steady Frame)
Δp	Wall Pressure Deviation from Average / Pressure Drop in RV
ECL	Ecole Centrale de Lyon
EO	Engine Order
λ	Acoustic Wavelength
LMFA	Laboratoire de Mecanique des Fluides et d'Acoustique
$m_{red,in}$	Reduced Inlet Mass Flow
N105%	Shaft Speed; 105% of Design Speed
NSV	Non Synchronous Vibration
OGV	Outlet Guide Vanes (Stator)
ΩR	Rotor Tip Speed
$p_{dyn,in}$	Dynamic Pressure at Stage Inlet
p_{in}	Static Wall Pressure upstream Rotor Leading Edge (unsteady)
p_{out}	Static Wall Pressure at Stage Exit (unsteady)
$p_i * p_j$	Cross Correlation of Two Sensor Signals, Wall Pressure or Strain Gauge
SP	Shock Position Relative to Blade [% Rotor Pitch]
σ	Standard Deviation
$\bar{\sigma}(p_1)$	Average Pre-Stall Standard Deviation of Unsteady Wall Pressure
SG	Strain Gauge Signal (Rotor Attached Vibration Measurement)
\bar{SG}_{10}	Ensemble Average of last 10 Revolutions of Strain Gauge Signal
SG_{Norm}	Average Amplitude of Blade Mode 1 During Rotating Stall
t	Time, Relative to First Stall Cell Occurrence
Θ	Circumferential Sensor Position
UHBR	Ultra High Bypass Ratio

References

- [1] Camp, T. R., and Day, I. J., 1998. "A study of spike and modal stall phenomena in a low-speed axial compressor". *ASME J. Turbomach.*, **120**(3), pp. 393–401.
- [2] Moore, F., 1984. "A Theory of Rotating Stall of Multistage Axial Compressors: Part I-Small Disturbances". *ASME J. Eng. Gas Turbines Power*, **106**(2), pp. 313–320.
- [3] Moore, F., 1984. "A Theory of Rotating Stall of Multistage Axial Compressors: Part II-Finite Disturbances". *ASME J. Eng. Gas Turbines Power*, **106**(2), pp. 321–326.
- [4] Moore, F., 1984. "A Theory of Rotating Stall of Multistage Axial Compressors: Part III-Limit Cycles". *ASME J. Eng. Gas Turbines Power*, **106**(2), pp. 327–334.
- [5] McDougall, N., Cumpsty, N., and Hynes, T., 1990. "Stall Inception in Axial Compressors". *ASME J. Turbomach.*, **112**(1), pp. 116–123.
- [6] Garnier, V., Epstein, A., and Greitzer, E., 1991. "Rotating Waves as a Stall Inception Indicator in Axial Compressors". *ASME J. Turbomach.*, **113**(2), pp. 290–301.
- [7] Tryfonidis, M., Etchevers, O., Paduano, J., Epstein, A., and Hendricks, G., 1995. "Pre-Stall Behaviour of Several High-Speed Compressors". *ASME J. Turbomach.*, **117**(1), pp. 62–80.
- [8] Bright, M. M., Qammar, H. K., and Leizhen, W., 1999. "Investigation of Pre-stall Mode and Pip Inception in High-Speed Compressors Through the Use of Correlation Integral". *ASME J. Turbomach.*, **121**(4), pp. 743–750.
- [9] Jackson, A., 1986. "Stall Cell Development in an Axial Compressor". *ASME J. Turbomach.*, **109**(4), pp. 492–498.
- [10] Day, I., 1993. "Stall Inception in Axial Flow Compressors". *ASME J. Turbomach.*, **115**(1), pp. 1–9.
- [11] Young, A., Day, I., and Pullan, G., 2013. "Stall warning by blade pressure signature analysis". *ASME J. Turbomach.*, **135**(1), p. 11033.
- [12] Inoue, M., Kuroamaru, M., Tanino, T., and Furukawa, M., 2000. "Propagation of multiple short-length-scale stall cells in an axial compressor rotor". *ASME J. Turbomach.*, **122**(1), pp. 45–54.
- [13] März, J., Hah, C., and Neise, W., 2002. "An experimental and numerical investigation into the mechanisms of rotating instability". *ASME J. Turbomach.*, **124**(3), p. 367.
- [14] Hah, C., 2016. "Effects of double-leakage tip clearance flow on the performance of a compressor stage with a large rotor tip gap". In *ASME Turbo Expo 2016: Turbomachinery Technical Conference and Exposition*, p. V02AT37A005.
- [15] Mailach, R., Lehman, I., and Vogeler, K., 2018. "Rotating Instabilities in an Axial Compressor Originating From the Fluctuating Blade Tip Vortex". *ASME J. Turbomach.*, **123**(3), pp. 453–460.
- [16] Kielb, R. E., Barter, J. W., Thomas, J. P., and Hall, K. C., 2003. "Blade excitation by aerodynamic instabilities: A compressor blade study". In *ASME Turbo Expo 2003*, collocated with the 2003 International Joint Power Generation Conference, pp. 399–406.
- [17] Brandstetter, C., Juengst, M., and Schiffer, H.-P., 2018. "Measurements of Radial Vortices, Spill Forward, and Vortex Breakdown in a Transonic Compressor". *ASME J. Turbomach.*, **140**(6), pp. 061004–061004–14.
- [18] Pullan, G., Young, A. M., Day, I. J., Greitzer, E. M., and Spakovszky, Z. S., 2015. "Origins and structure of spike-type rotating stall". *ASME J. Turbomach.*, **137**(5), pp. 51007–51011.
- [19] Yamada, K., Kikuta, H., Iwakiri, K.-i., Furukawa, M., and Gunjishima, S., 2013. "An explanation for flow features of spike-type stall inception in an axial compressor rotor". *ASME J. Turbomach.*, **135**(2), p. 21023.
- [20] Hendricks, G., Bonnaire, L., Longley, J., Greitzer, E., and Epstein, A., 1993. "Analysis of rotating stall onset in high speed axial flow compressors". In *29th Joint Propulsion Conference and Exhibit*, Monterey, CA.
- [21] Wilson, M. J., Imregun, M., and Sayma, A. I., 2006. "The Effect of Stagger Variability in Gas Turbine Fan Assemblies". *ASME J. Turbomach.*, **129**(2), pp. 404–411.
- [22] Schreiber, J., Paoletti, B., and Ottavy, X., 2016. "Observations on Rotating Instabilities and Spike Type Stall Inception in a High-Speed Multistage Compressor". *International Journal of Rotating Machinery*, **2017**, pp. Article ID 7035870 – 11 pages.
- [23] Greitzer, E., 1976. "Surge and Rotating Stall in Axial Flow Compressors-Part I and II". *ASME J. Eng. Gas Turbines Power*, **98**(2), pp. 190–211.
- [24] Day, I., 1994. "Axial Compressor Performance During Surge". *J. Propulsion and Power*, **10**(3), pp. 329–336.
- [25] Courtiade, N., and Ottavy, X., 2013. "Study of the Acoustic Resonance Occurring in a Multistage High-Speed Axial Compressor". *Proceedings of the Institution of Mechanical Engineers, Part A: J. Power and Energy*, **227**(6), pp. 654–664.
- [26] Lu, Y., Green, J., and Vahdati, M., 2018. "Effect of Geometry Variability on Fan Performance and Aeromechanical Characteristics". In *Proceedings of the 15th International Symposium on Unsteady Aerodynamics, Aeroacoustics and Aeroelasticity of Turbomachines*, Oxford, UK.
- [27] V. Srinivasan, A., 1980. "Influence of mistuning on blade torsional flutter". *NASA CR-165137/1*.
- [28] Castanier, M., and Pierre, C., 2002. "Using Intentional Mistuning in the Design of Turbomachinery Rotors". *AIAA Journal*, **40**(10), pp. 2077–2086.
- [29] Kielb, R. E., Feiner, D., Griffin, J. H., and Mizakozawa, T., 2007. "The Effect of Unsteady Aerodynamic Asymmetric Perturbations on Flutter". In *Proceedings of the ASME Turbo Expo 2007*, pp. 649–654.
- [30] Corral, R., and Martel, C., 2012. "Mistuning effects on flutter margin". *NATO RTO-EN-AVT-207*.